2002

Aftershocks and Pore Fluid Diffusion Following the 1992 Landers Earthquake

William Bosl
University of San Francisco, wjbosl@usfca.edu

A Nur

Recommended Citation
Bosl, W. J., and A. Nur, Aftershocks and pore fluid diffusion following the 1992 Landers earthquake, J. Geophys. Res., 107(B12), 2366, doi:10.1029/2001JB000155, 2002.

Aftershocks and pore fluid diffusion following the 1992 Landers earthquake

W. J. Bosl and A. Nur

Geophysics Department, Stanford University, Stanford, California, USA

Received 23 November 1999; revised 7 November 2001; accepted 13 November 2002; published 26 December 2002.

[1] We model the evolution of regional stress following the 1992 Landers earthquake in order to test the importance of pore fluid flow in producing aftershocks. Rising fluid pressure due to pore fluid flow and the resulting Coulomb stress changes were found to be strongly correlated with the time and location of aftershock events. Regional aftershock frequencies computed by integrating pore pressure decay rates also agreed quite well with aftershock data. Calculations show that regions of rising postseismic poroelastic Coulomb stress overlap considerably with regions of positive coseismic Coulomb stress. Thus pore fluid flow, which affects pore pressure within faults and causes regional poroelastic stress evolution following earthquakes, gradually evolves the initial coseismic stress changes. Together these changes provide a reasonable physical mechanism for aftershock triggering which agrees with data for the 1992 Landers earthquake. *INDEX TERMS:* 8164 Tectonophysics: Evolution of the Earth: Stresses—crust and lithosphere; 7209 Seismology: Earthquake dynamics and mechanics; 7260 Seismology: Theory and modeling; 7230 Seismology: Seismicity and seismotectonics; 8123 Tectonophysics: Dynamics, seismotectonics; *KEYWORDS:* aftershocks, seismology, earthquakes, tectonics, poroelasticity

Citation: Bosl, W. J., and A. Nur, Aftershocks and pore fluid diffusion following the 1992 Landers earthquake, *J. Geophys. Res.*, *107*(B12), 2366, doi:10.1029/2001JB000155, 2002.

1. Introduction

[2] The physical mechanism responsible for aftershocks remains an enigma. They are clearly associated with a preceding seismic event, and their spatial distribution is fairly well correlated with static (coseismic) Coulomb stress changes [*King et al.*, 1994; *Hardebeck et al.*, 1998]. Yet all aftershocks do not happen immediately following an earthquake. Rather, aftershock frequency decays like a diffusive process [*Nur and Booker*, 1972]. The key and surprisingly difficult question here is the identification of the actual physical process that is responsible for the typical time dependence of aftershocks, and their delay following the main event. Two main types of physical processes may account for the time dependence of aftershocks. One is a general process of time-dependent weakening following a major stress change [*Dieterich*, 1994; *Rundle et al.*, 1999]. In this process, aftershock sites (faults) on or near the main shock fault that have been subject to high shear stress experience gradual weakening until they fail. The weakening may be attributed to various physical and chemical causes [*Dieterich*, 1994; *Gomberg and Davis*, 1996; *Scholz*, 1990], which may include pore pressure changes due to creep compaction [*Sleep*, 1995].

[3] *Gomberg et al.* [1997] evaluated a version of fault weakening based on the rate- and state-dependent friction law of *Dieterich* [1994] using a simple slider block model. They found that transient loading caused by a large event advanced the time at which future earthquakes (aftershocks) occurred. This follows from the sensitive dependence of the slider block dynamical equations on the time-dependent, nonlinear friction coefficients. *Gross and Kisslinger* [1997] used a version of the *Dieterich* [1994] rate and state friction law to fit an aftershock rate curve to aftershock events of the 1992 Landers earthquake. This theory is based on changes in the fault strength over time due to changes in the microscale contact surfaces. A better understanding of the details of these processes may allow more predictive, quantitative modeling to be carried out to test these ideas in a manner similar to this study. It is interesting to consider that pore fluids are likely to be involved in the chemical processes responsible for rate and state theories, in addition to mechanical processes that create contact surfaces. More comprehensive future simulations might include these effects. *Gomberg and Davis* [1996] studied triggered seismicity at The Geysers geothermal field in California and concluded that dynamic strains (such as might result from a large earthquake) do not simply nudge prestressed faults over a failure threshold earlier than they otherwise would have failed. Rather, their study indicates that several competing processes with different timescales are operating, some inhibiting and some promoting failure.

[4] A specific physical process that has been proposed to explain the changing strength of regional faults is the time-dependent adjustment of local pore pressure changes induced on and around the main fault by the main rupture, as proposed first by *Nur and Booker* [1972]. This theory

0148-0227/02/2001JB000155$09.00

considers the sudden change in fluid pressure that is induced by the regional elastic stress changes after the main shock rupture. To first order, the stress field caused by the earthquake dislocation is assumed to remain approximately constant while fluid diffusion causes pore pressure in the faults to slowly change. The rate of pore pressure change in regions of increasing pore pressure should then be proportional to the regional aftershock rate.

[5] The other type of process that may be involved in aftershock triggering is a change in the regional stress field. *Richter* [1958] suggested that time-dependent elastic changes in the crust were responsible for triggering aftershocks, noting that "aftershocks are due to elastic afterworking." Though the physical cause of the elastic afterworking is not specified, several specific mechanisms can now be identified, including viscoelastic relaxation in the lower crust [*Deng et al.*, 1998; *Savage and Prescott*, 1978] and poroelastic relaxation due to fluid pressure redistribution. The latter is related to pore pressure changes within the faults, but also contributes to postseismic changes in the regional stress field. Several studies have demonstrated a good correlation between coseismic stress changes and aftershocks [e.g., *Harris*, 1998]. This suggests that postseismic stress changes are likely to be related to coseismic stress changes in a complementary manner. *Jaume and Sykes* [1992] show that local normal stress changes will continue to evolve in the same direction as the initial stress as local pore pressure reequilibrates. (Actually, it is the mean or hydrostatic stress that changes in direct proportion to pore pressure; normal stress is related to the mean stress, but is affected by fault orientation.)

[6] If fluid (free water) is present in the upper to mid crust in tectonic areas, pore pressure change must be induced by the sudden change in the stress field due to a large earthquake. The decay of the induced local pore pressure is time-dependent and obeys known poroelastic diffusion laws. Since there are many clear examples to demonstrate that the crust behaves as a fluid-saturated poroelastic medium, not simply an elastic medium [*Roeloffs*, 1996], pore pressure effects must be considered in order to understand the time-dependent nature of postseismic processes, including aftershocks. It is reasonable to assume that both fault weakening and resional stress evolution both occur to some extent following large earthquakes. A number of processes may occur simultaneously. In this study we assigned reasonable parameters to the crust and carry out simulations in order to determine how significant poroelastic stress relaxation may be following large earthquakes. In our study, local pore fluid pressure within faults and regional stress changes due to fluid redistribution are both included as natural consequences following a major earthquake.

[7] *Li et al.* [1987] investigated the correlation between time-dependent poroelastic Coulomb stress and aftershocks for three earthquakes. Their study was inconclusive. Important limitations that are mentioned in that study included simplified fault slip models, analytical poroelastic solutions which cannot account for heterogeneous diffusivities, and inaccurate aftershock locations. Our research has shown that detailed representations of fault slip, both horizontally and vertically, can greatly affect the location of pore pressure increase or decrease. This paper attempts to overcome some of these previous limitations in modeling postseismic poroelastic diffusion and reexamine the role of poroelastic fluid pressure and stress evolution following a major earthquake for which considerable data are available.

[8] Aftershocks of the 1992 Landers earthquake are investigated here using simulations of coupled poroelastic diffusion. It was found that postseismic Coulomb stress changes ($\tau_p(t)$) caused by pore fluid diffusion and the resulting stress evolution correlate well with aftershock location data. As discussed by *Jaume and Sykes* [1992], poroelastic stress changes will tend to develop in the direction of the main shock stress perturbation. In this sense, pore fluids act as a shock absorber, mitigating the full strain effect of large earthquakes on the regional stress field. Over time, pore fluids flow in response to the initial stress and the crust relaxes to the undrained state. Postseismic poroelastic relaxation will tend to enhance the effects of the initial coseismic stress on regional faults. Pore fluid flow should therefore be considered an important contributing factor in aftershock triggering, causing changes to both the regional stress field as well as modifying the frictional strength of faults. The hypothesis that pore fluid diffusion causes significant crustal stress changes after an earthquake is consistent with theories that consider pore fluid movement following the Landers earthquake to be an important contributing factor to postseismic deformation [*Bosl and Nur*, 1998; *Peltzer et al.*, 1996, 1998].

[9] The physical significance of poroelastic deformation will be greatest near the fault zone, where stresses cause the largest changes in pore pressure. Pore pressure diffusion will thus be fastest and will have the largest magnitude near the fault (within perhaps 10 km). Farther away from the fault, other competing processes may be more important. This is consistent with studies of crustal deformation [*Bosl and Nur*, 1998; *Deng et al.*, 1998; *Peltzer et al.*, 1996, 1998].

2. Fault Mechanics and Poroelasticity

[10] We present here a brief review of linear, isothermal poroelasticity as it relates to crustal dynamics and seismic faulting.

2.1. Poroelastic Deformation

[11] Pore pressure diffusion for a single phase fluid in a porous medium is coupled to the mean stress in the medium. *Biot* [1956] first derived the equations for coupled poroelasticity. A thorough derivation and discussion of the thermoporoelastic equations are given by *Charlez* [1991] and *Bosl and Nur* [2000b]. Isothermal conditions with static, spatially heterogeneous material properties are assumed here. The time-dependent equations are formulated in terms of coupled pore pressure and mean stress. The evolution of these two variables in a poroelastic material are governed by two equations, a diffusion equation that derives from mass conservation and Darcy's law:

$$\beta\left(\frac{\partial p}{\partial t} + B\frac{\partial \sigma}{\partial t}\right) = \frac{\partial}{\partial x_i}\left(k_{ij}(x)\frac{\partial p}{\partial x_j}\right) \tag{1}$$

and an equilibrium equation that derives from strain compatibility conditions:

$$\frac{\partial^2}{\partial x_j^2}[Ap + \sigma] = 0, \tag{2}$$

where

$$\beta = \mu\phi(C_f + C_r), \tag{3}$$

$$A = \frac{2(\nu_u - \nu)}{B(1-\nu)(1+\nu_u)}, \tag{4}$$

$p = p_{\text{total}} - p_{\text{ref}}$ is the pore pressure deviation from a reference pressure (hydrostatic or preseismic, for example), $\sigma = \sigma_{kk}/3$ is the mean stress deviation from a reference mean stress state (that is, $\sigma = \sigma_{\text{total}} - \sigma_{\text{ref}}$), B is Skempton's coefficient, ν_u and ν are the undrained and drained Poisson's ratios, μ is the fluid viscosity, ϕ is the porosity, C_f and C_r are the fluid and rock compressibilities, respectively, and $k_{ij}(x)$ is the spatially variable permeability tensor. The common assumption of a constant scalar permeability is avoided here, since heterogeneous permeability is likely to be significant for studies of crustal deformation. The material property coefficients in our formulation remain in their correct position inside of spatial derivatives. If they are pulled out of the derivatives, as is common in the formulation of poroelasticity, then the use of spatially heterogeneous coefficients is will give incorrect results. Initial and boundary conditions for both pore pressure and mean stress are required to complete this set of equations.

[12] One difficulty in modeling flow in porous media, whether one is interested in the transport of contaminants in an aquifer, the flow of oil from a petroleum reservoir, or the diffusion of pore pressure following an earthquake, is determination of the permeability of the porous rocks. In faulted regions, the permeability structure may be quite heterogeneous [*Hickman et al.*, 1994]. Permeability in fault zones has been observed to be both anisotropic and asymetrically distributed [*Seeburger*, 1981]. Zones of low permeability provide a mechanism for transient pore pressure increase in a fault even when the pore pressure in the surrounding rock is decreasing through the Mandel-Cryer effect [*Bosl and Nur*, 2000a; see also *Cryer*, 1963]. For this present study, we will have to assume a simple, homogeneous permeability field, but note that much effort is expended by environmental and oil companies to determine the permeability of a reservoir because of its importance in controlling fluid flow. A conceptual model with more detailed and accurate representation of the actual permeability structure in the Landers region would yield a more realistic simulation of pore fluid diffusion effects, though we believe that the overall implications of this study would be the same.

[13] Elastic displacements and the resulting stress field induced by uneven pore pressure distribution in porous rocks may be computed from the Navier equations with pore pressure included as a forcing term. The equations for elastic displacement in terms of pore pressure are

$$\frac{\partial}{\partial x_i}\left[(\lambda + G)u_{k,k}\right] + \frac{\partial}{\partial x_k}\left(Gu_{i,k}\right) = \frac{\partial}{\partial x_i}(\alpha p), \tag{5}$$

where u_i are the three components of the displacement vector, λ is the usual Lame coefficient, and G is the shear modulus. Both of these may be spatially variable in this formulation. The Biot-Willis parameter, α, is a function of Skempton's coefficient and the drained and undrained Poisson's ratios: $\alpha = 2(\nu_u - \nu)/[B(1 - 2\nu)(1 + \nu_u)]$. The right side of equation (5) is expressed in terms of the deviation of the pore pressure from a reference value, $p = p_{\text{total}} - p_{\text{ref}}$. Thus the state of stress and pore pressure just before the earthquake event is the reference state. From now on, p will be used to represent the change in pore pressure from the preseismic reference state. Gravitational forces have not been included here, but may be included as another body force.

[14] Strain and stress can be computed from the displacement field in the usual way from derivatives of the displacement field and the elastic constitutive law:

$$\begin{aligned} \varepsilon_{ij} &= \frac{1}{2}\left(\frac{\partial u_i}{\partial u_j} + \frac{\partial u_j}{\partial u_i}\right) \\ \sigma_{ij} &= 2G\varepsilon_{ij} + \lambda\delta_{ij}\varepsilon_{kk}, \end{aligned} \tag{6}$$

where λ is the Lame parameter. We note here that the mean stress deviation in equation (1) will have the same value as the mean stress computed from equations (5) and (6) and $\sigma = \sigma_{kk}/3$. The redundant independent variable σ is introduced for computational efficiency, since it allows equations (1) and (2) to be solved as a coupled system of two unknowns. Equations (5) can then be solved as an elliptic system of three unknowns only at desired time intervals, using the already computed pore pressure. The alternative would be to solve equations (1) and (5) as a fully coupled system of four unknowns at every time step.

[15] Material properties chosen for the Landers region are shown in Table 1. Values were taken from *Mavko et al.* [1998] and *Wang* [1993]. The poroelastic equations described above can be solved numerically by finite element discretization. Mathematical and algorithmic details are described more fully by *Bosl and Nur* [2000b]. The code used for computations was written using the Diffpack numerical libraries www.nobjects.com), which allows rapid code development using well-tested and robust mathematical components. The linear system derived from the finite element discretization was solved using a stabilized biconjugate gradient (BiCGStab) method with relaxed incomplete LU (RILU) decomposition. Petrov-Galerkin elements are specified (helpful in controlling numerical diffusion), though for this problem the weighting functions and basis

Table 1. Crustal Material Properties Used in the Numerical Simulation of Poroelastic Stress Evolution

Parameter	Symbol	Value
Permeability	k_{ij}	(1,1,1) mD
Fluid viscosity	μ	0.001 Pa s
Porosity	ϕ	0.02
Fluid bulk modulus	$1/C_f$	2 GPa
Rock bulk modulus	$1/C_r$	44 GPa
Lambda	λ	29 GPa
Shear modulus	G	22 GPa
Drained Poisson ratio	ν	0.25
Undrained Poisson ratio	ν_u	0.31
Skempton's coefficient	B	0.8
Derived quantities		
$\mu\phi\,(C_f + C_r)$	β	1.0×10^{-14}
$\frac{2(\nu_u-\nu)}{B(1-\nu)(1+\nu)}$	A	0.13
Biot-Willis $\frac{3(\nu_u-\nu)}{B(1-2\nu)(1+\nu)}$	α	0.30

functions were the same, yielding the standard Galerkin formulation. BiCGStab is appropriate for nonsymmetric linear systems which may result when heterogeneous, anisotropic material properties are used. The code structure was derived from the convection-diffusion class described by *Langtangen* [1999, p. 403 ff]. The solver for equation (5) used standard Galerkin elements and ILU preconditioning; the code was derived from *Langtangen* [1999, p. 367 ff].

2.2. Rock Strength and the Coulomb Criterion

[16] A common measure of the static frictional strength of a fault is the empirical Coulomb fracture criterion. The Coulomb stress is the shear stress on a fault minus the frictional strength of the fault, expressed mathematically by

$$\tau_c \equiv \sigma_s + \mu_s(\sigma_n + p), \tag{7}$$

where τ_c is the Coulomb stress, σ_s and σ_n are the shear and normal stresses with respect to a specified fault plane, and p is the fluid pressure in the fault [*King et al.*, 1994; *Harris*, 1998]. We use the convention that compressive stresses are negative. A fault tends to fail when $\tau_c > 0$. Whereas the mean stress is isotropic, σ_n depends on the local stress field and the orientation of the fault of interest. Though the orientation of individual faults is usually unknown in a region, the average orientation of many faults in a region can often be inferred. In order to compute statistics for aftershocks following a large earthquake, a common assumption is that fault orientation is well distributed at every location. Those faults that are oriented so as to maximize the Coulomb stress will be most likely to fail [*King et al.*, 1994]. If focal mechanisms for aftershocks can be determined, then the ambiguity in fault orientation can be reduced to two conjugate planes. This is appropriate for a study of physical mechanisms that may be involved in earthquake triggering. *Hardebeck et al.* [1998] have done this for aftershocks of the 1992 Landers earthquake. To predict aftershock locations from poroelastic forward models, it will be necessary to make assumptions about fault orientation. Optimal orientation for failure or orientations based on field observations may be more useful for this purpose.

[17] It is common to assume that pore pressure is simply a linear function of the local mean stress. This simplification implies that the undrained condition is applicable. A poroelastic medium is said to be in the undrained state when the stress modification that results from a dislocation (or other suddenly imposed stress) occurs so quickly that fluids in the pores are essentially stationary and do not flow significantly. Mathematically, undrained pore pressure implies that

$$p = -B\sigma, \tag{8}$$

where σ is the mean stress and the proportionality constant B is Skempton's coefficient. Here, we assume negative stress is compressive. Skempton's coefficient is an empirically determined constant that quantifies the fraction of a compressive stress on a porous rock that is transferred to the pore fluid. *Wang* [1993] gives values for B in crustal rocks in the approximate range 0.55 to 0.9. If fault-normal compression is independent of fault orientation, then $\sigma \approx \sigma_n$. This allows an effective friction coefficient to be defined, $\mu_e = \mu_f(1 - B)$, which incorporates pore pressure into an effective Coulomb stress:

$$\tau_e \equiv \tau + \mu_e\sigma_n. \tag{9}$$

We define the static Coulomb stress change as the Coulomb stress step, τ_e, of the undrained crust, which is instantaneous on the timescale considered here. On timescales over which aftershocks occur, the undrained assumption does not hold [*Jaume and Sykes*, 1992; *Peltzer et al.*, 1998], which suggests that the time-dependent development of the Coulomb stress should be examined more closely.

[18] For clarity, in Table 2 we define some terminology here that will be used throughout the rest of this paper. We note here that the time-dependent changes to Coulomb stress in this paper are due entirely to poroelastic stress changes. That is, $\partial\tau(t)/\partial t = (\partial\tau_0/\partial t) + [\partial\tau_p(t)/\partial t] = \partial\tau_p(t)/\partial t$, since the static Coulomb stress does not change with time.

Table 2. Symbols Used for Stress and Pore Pressure in Equations

Parameter	Definition
τ_0	static Coulomb Stress due to the initial dislocation
$\tau_p(t)$	postseismic Coulomb stresschange due to poroelastic relaxation
$\tau(t) = \tau_0 + \tau_p(t)$	total Coulomb stress
$p(t)$	pore pressure

3. Aftershock Rates

[19] The decay rate of aftershock frequency is well established and behaves like a diffusive process [*Nur and Booker*, 1972; *Scholz*, 1990]. This is a strong indication that a time-dependent physical process is at work that has diffusive-like dynamics.

3.1. Nur and Booker Hypothesis

[20] Pore fluid diffusion was first proposed by *Nur and Booker* [1972] as the time-dependent process responsible for causing aftershocks. Their idea was relatively simple: when an earthquake occurs, there is an almost instantaneous modification to the regional stress field. The change in strength of a fault (or rock), which they considered, determined experimentally by *Hubbert and Rubey* [1959], was given by

$$\Delta S = -\mu_f(\sigma + p) \tag{10}$$

where μ_f is the coefficient of internal friction or simply the frictional strength, σ is the mean stress, and p is the pore pressure in the fault. In this formulation, compressive stresses are negative; this convention is followed throughout this paper. Aftershocks will occur on faults where the shear stress exceeds the strength of the fault. Immediately following an earthquake, the pore pressure is changed by an amount proportional to the mean stress induced by the earthquake: $p = -B\sigma$. In many studies of poromechanics, a first-order assumption is that the Skempton's coefficient $B \approx 1$. After the earthquake, pore fluids will flow from regions of high pressure (compressional regions) to regions of low pressure (dilatational regions). The applied mean stress field will remain approximately constant, so the strength of the fault will change over time in proportion to

the amount of pore pressure change. The number of aftershocks, according to this theory, should be proportional to the time rate of change of pore pressure integrated over the region where the pore pressure is increasing after the earthquake, because ΔS decreases correspondingly in these regions. That is, aftershocks will tend to occur primarily in regions of coseismic dilatation.

[21] *Nur and Booker* [1972] postulated that the frequency of aftershocks in a volume near the main shock was proportional to the time derivative of the local pore pressure. The total number of aftershocks per unit time is

$$\frac{dN}{dt} = \frac{1}{\alpha} \int \frac{\partial p}{\partial t} dv. \tag{11}$$

The proportionality constant α is equal to the increase in pore pressure between successive fractures multiplied by some appropriate volume. The integration is carried out over the volume where pore pressure is increasing. In regions where pore pressure is decreasing, aftershocks will tend to be suppressed and will therefore not contribute to aftershock production.

3.2. Aftershock Frequency and the Coulomb Stress

[22] The aftershock frequency result found by *Nur and Booker* [1972] considered the effects of pore pressure on fault strength only. A result similar to equation (11) can also be derived by replacing the pore pressure, p, with total Coulomb stress, $\tau(t)$. The total Coulomb stress, however, includes not only changes to the pore pressure within the fault, but also changes in the stress field surrounding the fault.

[23] There is some evidence to suggest that changes to the shear stress caused by pore fluid diffusion are significant. *Booker* [1974] showed that in the case of a simple edge dislocation, shear stresses along a fault may be strongly coupled to pore pressure and can change appreciably over time due to fluid diffusion. *Li et al.* [1987] showed that pore fluid diffusion results in slow rotation of the stress shadow caused by an edge dislocation. These suggest that regional poroelastic stress changes (which affect the shear stress term in equation (9)) should be considered as well as local pore pressure changes within faults (p in equation (9)).

[24] It is clear from the coupled poroelastic equations that pore pressure and stress both change with time as fluids diffuse in a porous medium. Just before an earthquake, pore fluid is in a reference state. A sudden change in the pore pressure distribution is induced by the initial dislocation stress and can be computed from equation (8). The pore pressure, p, used throughout this paper refers to the pore pressure change introduced by the main shock dislocation. Stress changes that result from pore fluid diffusion must satisfy the compatibility equation (equation (2)). If boundary conditions are imposed such that the pressure perturbation is zero far from the fault, a simple solution to equation (2) is $Ap + \sigma = 0$. Note that σ is the change in the stress field due to pore fluid diffusion; its magnitude is relative to the initial stress induced by the coseismic dislocation. Then

$$\frac{\sigma}{\sigma_{\text{init}}} = \frac{\nu_u - \nu}{(1-\nu)(1+\nu_u)}. \tag{12}$$

The postseismic mean stress change induced by pore pressure relaxation will have the same sign as the initial mean stress change. That is, mean stress will continue to increase or decrease where the initial mean stress caused by the dislocation increased or decreased, respectively.

[25] For $(\nu_u, \nu) = (0.28, 0.25)$, which is reasonable for low porosity rocks, σ will be $\sim$3% greater than the initial coseismic mean stress. Taking more extreme values that might be typical for the upper crust when fractures are present, $(\nu_u, \nu) = (0.31, 0.15)$, we find that $\sigma \sim 14\%$ greater than σ_{init}. Coulomb stress changes on individual faults will depend upon the orientation of the fault. These estimates of mean stress change give some indication of the magnitude of poroelastic Coulomb stress changes that might be expected following large earthquakes.

4. Aftershocks of the 1992 Landers Earthquake Sequence

[26] In order to test our theories about aftershock triggering, we chose to look at the 1992 Landers earthquake sequence. The 1992 Landers earthquake was a large and well-documented earthquake. The faults that ruptured in the Landers earthquake are located in the Mojave Block of southeastern California, which is dominated by northwest trending, right-lateral strike-slip faults.

[27] The Landers earthquake was preceded by 2 months of intense seismic activity in the region south of the main shock fault trace [*Yeats et al.*, 1997, pp. 225–227]. The largest of these foreshocks was the M6.1 Joshua Tree earthquake which occurred on 23 April 1992. Aftershocks of the Joshua Tree earthquake migrated northward in the 2 months between the Joshua Tree and Landers earthquakes. This activity continued to migrate to the vicinity of the Landers hypocenter until only hours before the main shock.

[28] A major aftershock occurred on the Big Bear fault $\sim$3 hours after the Landers earthquake and 40 km to the west of the Landers rupture. The Big Bear earthquake presumably had a different orientation and slip than the Landers earthquake; it was roughly conjugate to the Landers event and thus optimally oriented for failure following the Landers main shock [*King et al.*, 1994]. The Landers surface rupture produced right-lateral displacement over a total rupture length of $\sim$85 km. Average slip of 2–4 m was measured along the surface and the moment magnitude was determined to be $M = 7.3$.

4.1. Slip Models and Fluid Flow Simulation

[29] The initial stress distribution is computed from the fault parameters of *Hudnut et al.* [1994], who used geodetic and surface rupture data to produce a detailed horizontal slip model of the Landers earthquake. The model consists of 27 vertical faults of varying length and strike. Each plane extends uniformly to a depth of 10 km. The surface pattern is shown in Figure 1. This model honors the geology of the observed surface rupture of the Landers earthquake, though it is limited by its assumption of uniform vertical slip. *Wald and Heaton* [1994] and *Cohee and Beroza* [1994] give alternative fault models that have a simpler horizontal representation of the Landers event but variable slip with depth. These consist of three vertical faults, composed of a total of 186 subfaults, that are colinear with the three main faults.

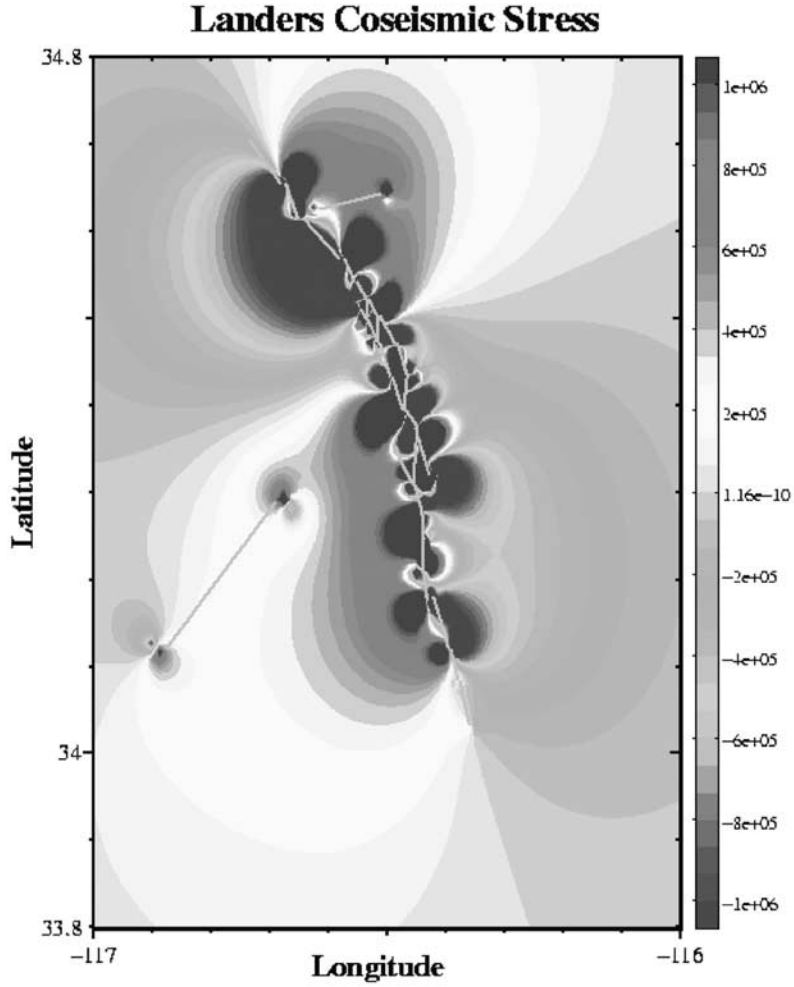

Figure 1. Coseismic mean stress field computed from *Hudnut et al.* [1994] slip model. Fault trace is superimposed on the mean stress image. Negative mean stress is compressive. Initial pore pressure distribution is computed directly from this. See color version of this figure at back of this issue.

[30] We use this model to compute the coseismic mean stress that would be produced by the earthquake. From this, the pore pressure changes due to the mean stress are computed from the undrained condition (equation (8)).

[31] This condition applies only at the time of fault slip, before the fluid has time to diffuse appreciably. Subsequent fluid flow is then simulated by solving the coupled poroelastic equations as discussed in section 2.1. It should be noted that although the slip model of *Hudnut et al.* [1994] has considerable horizontal detail, it does not include vertical variability. Although our numerical model is fully three dimensional, the simulation results are quasi two dimensional because of the vertical homogeneity of the material properties and the fault model.

[32] The domain we studied is the region bounded by longitude -117.0° to -116.0° and latitude 33.8° to 34.8°, a region approximately 92 km by 111 km. The rate at which pore pressure decays is controlled by the permeability of the crust. In the present study, permeability was assumed to be homogeneous and isotropic over the entire region. This zeroth-order calculation allows us to estimate the magnitude of the poroelastic effect on aftershock activity. It is well-known that permeability in faulted regions is anisotropic and heterogeneous. *Jaume and Sykes* [1992] point out that field studies of ancient faults of the San Andreas fault system show signs of anisotropic permeability and the effects of fluid flow in the fault. More detailed simulations will require detailed lithologic characterization of the Landers region in the manner now used for aquifer and reservoir simulations. Fluid and elastic parameters are shown in Table 1.

[33] Figure 1 shows the static (coseismic) pore pressure distribution, τ_0, that was computed from Hudnut's fault model, which is superimposed. Recall that coseismic pore pressure and mean stress are directly related by equation (8). The coseismic pore pressure distribution is the change in pore pressure induced by the earthquake dislocation, as discussed in sections 2.1 and 3.2. Initial stresses were computed using the elastic dislocation formulas of *Larsen* [1991]. The grid uses 4 km $\times$ 4 km $\times$ 5 km cells and appears to have enough resolution to capture most of the spatial variability of the pore pressure along the fault.

[34] We compared aftershock locations with static coseismic Coulomb stress changes using both the *Hudnut et al.* [1994] and *Wald and Heaton* [1994] models. The focal mechanisms for all events following the main shock determined by *Hardebeck et al.* [1998] were used to compute

Coulomb stresses at the location of aftershock events. As discussed in section 2.2, we compute the Coulomb stress on both (conjugate) fault planes. If either computed Coulomb stress is positive, the Coulomb stress at this location and time is taken to be positive. Unlike previous studies, we do not exclude events near the fault zone. We found that the fraction of events that occur where coseismic stress is positive is similar for both the *Wald and Heaton* [1994] and *Hudnut et al.* [1994] models, with ~76% of events occurring where the coseismic static stress, τ_0, was positive (see Figure 2). Since the *Hudnut et al.* [1994] model honors surface geology and variability more accurately, we believe that it gives more accurate simulation results near the fault, where both pore pressure $p(t)$ and Coulomb stress will experience the greatest postseismic changes and is also where most aftershocks occur. All of the results presented henceforth will be based on this model.

4.2. Regional Aftershock Frequency

[35] Regional aftershock frequencies according to the Nur and Booker hypothesis may be computed from simulated pore pressures at selected times by integrating numerically the time rate of change of pore pressure over a defined volume:

$$\frac{1}{c}\int_{\Omega^+}\left(\frac{\partial P}{\partial t}\right)dx \approx \frac{1}{c}\sum_{i=1}^{N}\frac{P(t_n)-P(t_{n-1})}{\Delta t}v_i \qquad (13)$$

where Ω^+ is the domain of interest where pore pressure is increasing, v_i is the volume of the ith cell, and the summation is over all N cells in the domain. The aftershock domain, Ω, used in for all figures in this paper, is outlined in yellow in the regional map in Figure 3. In the integration, only grid cells where pore pressure is increasing at the time of the aftershock event (the original hypothesis assumed that pore pressure was either increasing or decreasing uniformly for all time following an earthquake; here we do not have to assume this) are included in Ω^+; c is a scaling factor which relates the change in pore pressure to the aftershock frequency. It is related to the density of faults in region.

[36] Figure 4 shows actual aftershock frequency data and the computed frequency based on the pore pressure diffusion hypothesis. This was accomplished by solving equation (1) numerically as described in section 2.1, yielding $p(t)$ at each time step. At each time step, the pore pressure change from the previous time step was computed at every grid point. The pore pressure changes were then integrated over the entire spatial domain using equation (13).

[37] The scaling parameter $c = 8$ was determined empirically by fitting the theoretical curve to the aftershock data. The theoretical curve is approximately level until roughly 10 days, when it begins to follow a linear decline on the log-log plot. This corresponds approximately to the actual data, which excludes aftershocks with magnitude less than 2.0. In the analytical solution shown in Nur and Booker's original work, the theoretical pore pressure diffusion curve is a straight line on log-log axes. This can occur only if the pore pressure is a delta function; that is, the analytic solution presumes infinite pore pressure at time 0 in an infinitely small volume, which is not physically realistic. Numerically, the pore pressure assumes a finite value that is controlled by the finite grid size. This corresponds physically to the fact that an elastic dislocation model fails when the theoretical elastic stress exceeds the strength of the rock. Pore pressure or coseismic stress have a finite limit in real rocks.

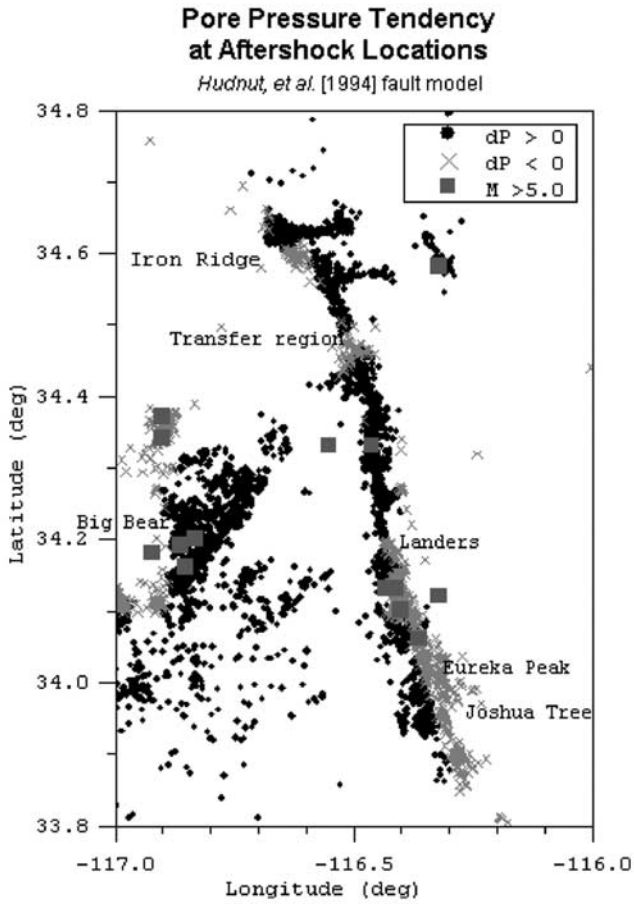

Figure 2. Locations of all $M > 2.0$ aftershocks in the 1-year period following the Landers earthquake are shown. Black dots indicate events that occur where the coseismic Coulomb stress, τ_0, is positive and red crosses indicate events where $\tau_0 < 0$. Large aftershocks ($M > 5.0$) are shown as blue squares.

[38] The predicted aftershock frequency curve corresponds quite well to the actual aftershock frequency data. Calculation of aftershock frequency curves for subdomains of the entire regions surrounding the Landers earthquake also agreed reasonably well with data. However, a much better test of the theory is to look at pore pressure tendency and Coulomb stress at the locations of individual aftershock events.

4.3. Coulomb Stress and Pore Pressure Tendency

[39] To directly test the hypothesis that aftershocks will tend to occur where pore pressure is increasing, the location in space and time of each aftershock in the first year following the main earthquake were read into our pore fluid diffusion model during program execution. On each day of the simulation, the pore pressure trend, Coulomb stress on that day, and the initial Coulomb stress at the location of each aftershock was calculated. Coulomb stresses were computed using focal mechanisms that we determined from

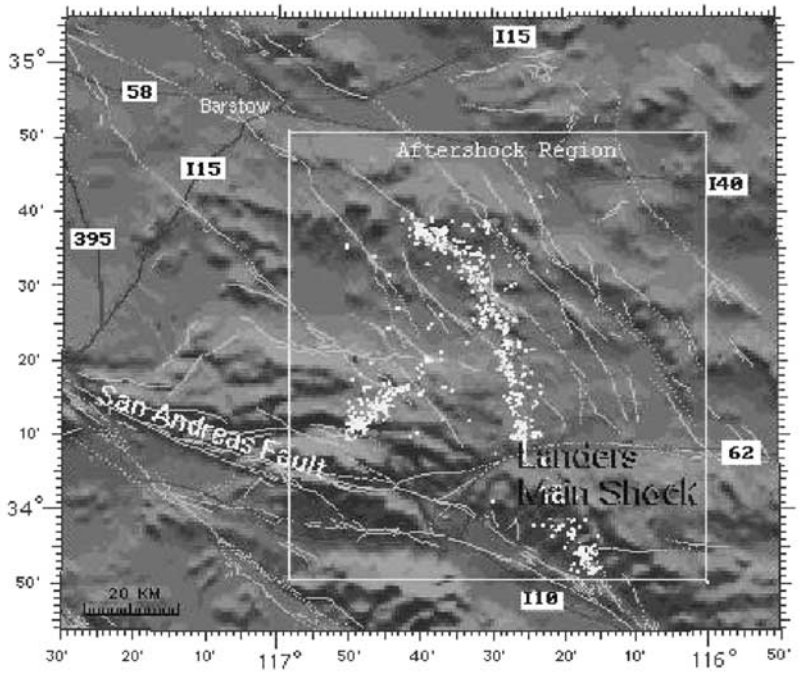

Figure 3. Sketch of the Mojave region where the Landers earthquake occurred. The yellow box outlines the region over which aftershock events were counted for this study. See color version of this figure at back of this issue.

seismic data reported by *Hardebeck et al.* [1998] (data kindly supplied in digital form by E. Hauksson, California Institute of Technology). Results for all aftershocks of $M >$ 2.0 in the one year period following the Landers earthquake are shown (Figures 2, 5, and 6) as well as for aftershocks of the Joshua Tree "prequake" that occurred before the Landers earthquake, 23 April through 28 June 1992 (Figure 7). There were 2575 aftershocks included in our study between the 23 April Joshua Tree main shock and the 28 June 1992 Landers earthquake and 7255 aftershocks in the year following the Landers earthquake. The Joshua Tree and Landers earthquakes were treated as separate events using separate calculations. This was required because our model can only be initialized at the start of a simulation by an

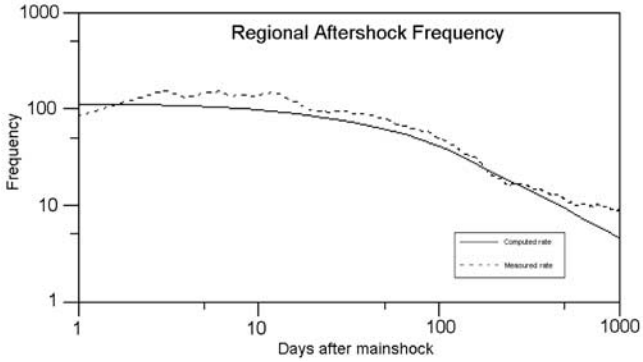

Figure 4. Regional aftershock frequency (events per day) following the 1992 Landers earthquake as a function of the days after the main shock. Dashed line is actual measurements. The solid line is the computed frequency based on the hypothesis of Nur and Booker.

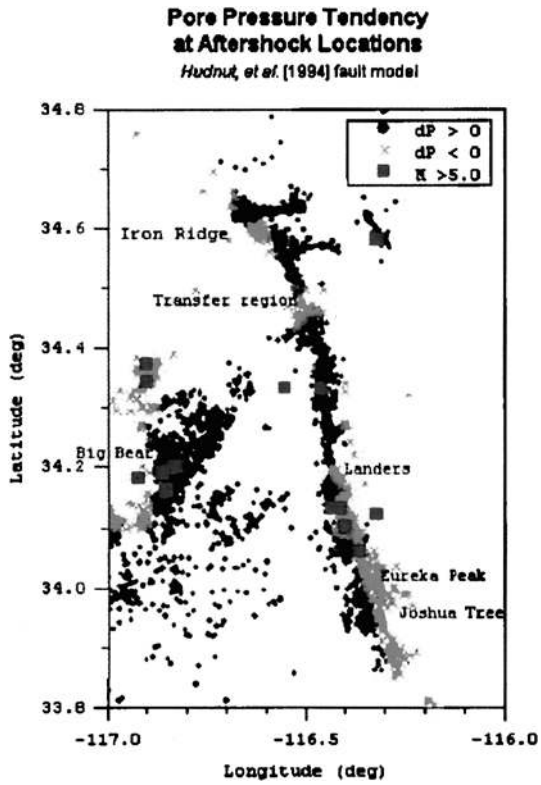

Figure 5. Locations of all $M > 2.0$ aftershocks in the 1-year period following the Landers earthquake are shown. Black dots indicate events that occur where the pore pressure has increased since the main shock, and red crosses indicate events where pore pressure has decreased. Large aftershocks ($M > 5.0$) are shown as blue squares. See color version of this figure at back of this issue.

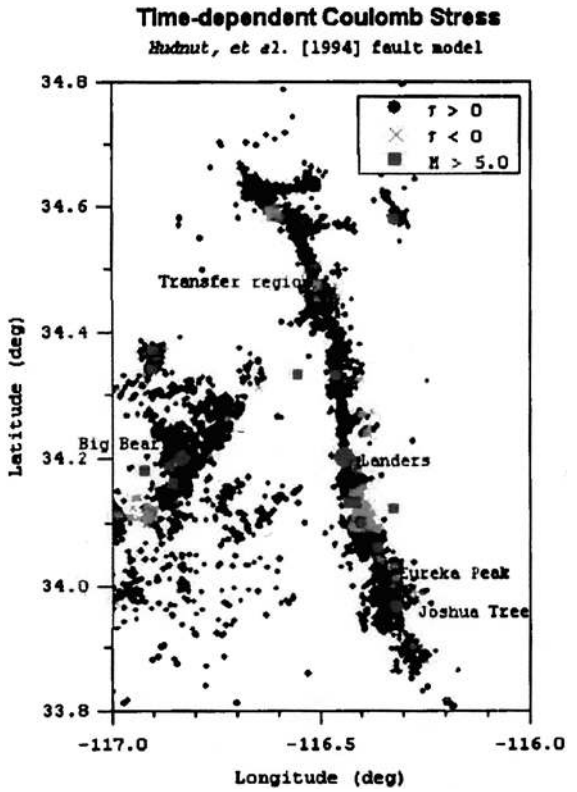

Figure 6. Locations of all $M > 2.0$ aftershocks in the 1-year period following the Landers earthquake are shown. Black dots indicate events that occur where the total Coulomb stress is positive, and red crosses indicate events where it is negative at the time of the event. Large aftershocks ($M > 5.0$) are shown as blue squares. Black dots ($\tau(t) > 0$) represent 86% of the aftershocks. See color version of this figure at back of this issue.

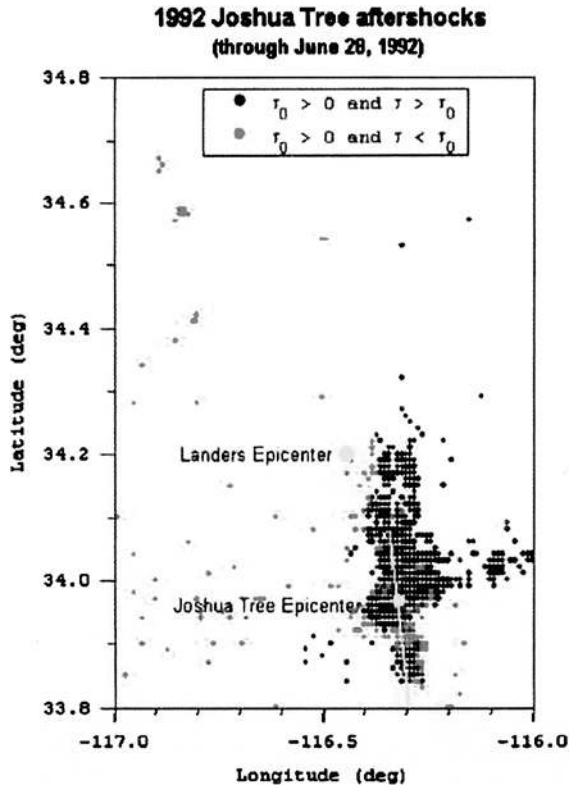

Figure 7. Locations of all $M > 2.0$ aftershocks in the 3-month period (23 April to 28 June) following the Joshua Tree earthquake are shown. Black dots indicate events that occur where the total Coulomb stress is positive, and red crosses indicate events where it is negative at the time of the event. Black dots ($\tau(t) > 0$) represent 95% of the aftershocks. See color version of this figure at back of this issue.

earthquake dislocation event. Future enhancements will allow earthquakes and aftershocks to alter the stress and pore pressure distributions during time integration of the poroelastic equations.

[40] Unlike other studies of the Landers earthquake sequence [*King et al.*, 1994; *Hardebeck et al.*, 1998], we included all events within the region bounded by [−117.0, −116.0] in longitude and [33.8, 34.8] in latitude and did not exclude events near the fault zone. Though this makes the results somewhat sensitive to the fault model, the *Hudnut et al.* [1994] fault model was thought to contain enough horizontal detail to allow this. Results are summarized in Table 3. These results show that the total Coulomb stress at most aftershock locations had risen since the main shock. Pore pressure was also rising at most aftershock locations. Note that total Coulomb stress can be rising at an aftershock location even if the pore pressure is not. This is particularly so off the ends of the fault where pore pressure is nearly zero, but the shear stress due to poroelastic relaxation is changing significantly. We note that if aftershocks within 5 km of the fault zone are excluded, the number of events occurring where the poroelastic Couloub stress is rising is somewhat higher.

[41] The mean change in Coulomb stress due to poroelastic relaxation for all aftershocks at the location and time of the event is greater than 1.5 bars (0.155 MPa) for Landers aftershocks and 0.4 bars (0.042 MPa) for aftershocks of the Joshua Tree earthquake which occurred before the Landers event. This seems to indicate that Coulomb stress changes due to postseismic fluid flow are a significant factor in causing the aftershocks. Though positive coseismic Coulomb stress is strongly correlated with aftershock locations, our results suggest that the continuing increase in Coulomb stress after the main shock is the physical explanation for the time delay in aftershock occurrence. The correlation between these two measures is not surprising, since regions of rising poroelastic Coulomb stress and regions of positive coseismic (dislocation) Coulomb stress overlap considerably [*Jaume and Sykes*, 1992; *Bosl and Nur*, 2000a].

[42] We also found that the fraction of aftershocks occurring where the total Coulomb stress is positive at the time of

Table 3. Summary of Simulation Results for Joshua Tree and Landers Aftershocks[a]

Event	$p(t)$ Rising	$\tau(t) > 0$ and $\tau(t) > \tau_0$	$\tau(t) > 0$	Mean $\tau_p(t)$ (for All Events)
Landers	62%	65%	87%	+0.155 MPa
Joshua Tree	72%	79%	(includes both events)	+0.042 MPa

[a]Refer to Table 2 for definitions of the various terms.

the event is significantly larger than when static coseismic Coulomb stress is considered. *King et al.* [1994] found that approximately three fourths of aftershocks more than 5 km from the fault zone were in regions of positive coseismic Coulomb stress, assuming faults were optimally oriented for failure. *Hardebeck et al.* [1998], using estimated focal mechanisms for each aftershock fault, found this figure to be ~85%, again for events farther than 5 km from the fault zone. We did not exclude aftershocks near the fault zone. Using the same focal mechanisms as *Hardebeck et al.* [1998], we found that 87% of the aftershocks from the Joshua Tree and Landers earthquakes, including events near the fault zone, occurred where the total Coulomb stress was positive, $\tau(t) > 0$, at the time of the event. We emphasize here that the significance of these results is that total Coulomb stress changes due to poroelastic relaxation are large enough to trigger aftershocks, particularly near the fault. Furthermore, our simulations indicate that most of the aftershocks do occur where the total Coulomb stress is increasing following the main shock. This hypothesis is not competing with the static Coulomb stress theory of aftershock triggering. Rather, it extends that theory by providing a physical mechanism to explain the time delay in the aftershock sequence.

[43] Note that the fault orientation used to compute the Coulomb stress is ambiguous. We assume that the Coulomb stress is positive when it is positive on either of the conjugate fault planes. *King et al.* [1994] followed this procedure when computing the Coulomb stress on optimally aligned faults. *Hardebeck et al.* [1998] point out that it may be more appropriate to count as positive only those aftershocks for which the Coulomb stress is positive on both planes and randomly count only 50% of those for which only one of the conjugate planes has a positive Coulomb stress. If this procedure had been followed, the percentages in columns two and three of Table 3 might decrease slightly. (*Hardebeck et al.* [1998] estimate that only 10% of the aftershocks will have differing Coulomb stresses on the conjugate planes, since the shear stress will be the same on each.) Since the pore pressure value does not depend on fault orientation, there is no such ambiguity when determining pore pressure change at aftershock locations.

[44] Figure 5 shows aftershock locations, using colored dots to indicated the pore pressure tendency. Clustering on the basis of pore pressure tendency appears to be even more pronounced than the clustering observed for initial Coulomb stress in Figure 2. It is significant that the aftershocks which do not agree with our hypothesis are not randomly scattered. This suggests that pore pressure changes alone are not the cause of aftershocks. They are primarily found in four distinct clusters where the faulting is particularly complex: in the transfer region between the Homestead Valley and Emerson faults, centered at −116.5°W, 34.5°N; northwest of the Big Bear fault; and south of the Landers/Johnson Valley fault, north of the Joshua Tree rupture site along the Emerson fault. There is evidence to suggest that the faulting in each of these locations may not be adequately represented in our slip model (or in other models).

[45] Figure 6 shows graphically the location of aftershocks where $\tau(t)$ is either positive or negative. Evidently, the Coulomb stress may be initially negative in some locations, but become positive as pore fluids are redistributed. The mean poroelastic Coulomb stress change from the main shock (Joshua Tree or Landers) to the time of the aftershock is also shown in Table 3. This gives an indication of how much the Coulomb stress is changing at aftershock locations. The changes are significantly large and positive, which is another indication that poroelastic stress changes are reasonable physical causes for aftershock occurence and time delay.

[46] Aftershocks of the Joshua Tree earthquake (or preshock) that occurred before the 28 June Landers earthquake also show the same pattern as aftershocks of the Landers earthquake. The majority of aftershocks occur where the total Coulomb stress is both positive and increasing at the time of the event (Figure 7). The computed poroelastic Coulomb stress tendency following the Joshua Tree event, at the site of the (future) Landers earthquake, was slightly decreasing. We note, however, that our fault model was a simple linear fault as shown in Figure 7. *Yeats et al.* [1997, p. 226] show that the Joshua Tree fault is not linear, but bends to the northeast at its northern end. If this is so, the epicenter of the Landers earthquake would clearly be in a dilational region where the pore pressure and poroelastic Coulomb stress would both be increasing.

5. Discussion

[47] The simulation results presented thus far seem to indicate that increasing Coulomb stress due to poroelastic relaxation may explain the time delay in aftershock occurrence. Not only do a majority of aftershocks occur where the Coulomb stress has increased and where pore pressure has increased, but those that do not agree with this theory are clustered and not randomly scattered. There are plausible physical explanations to account for the minority of aftershocks that occur in regions where the Coulomb stress or pore pressure has declined. Inadequate fault slip models, exclusion of large aftershocks in the calculation of the stress field, and material property heterogeneities are the most likely sources of error. Three clusters of aftershocks are of particular interest, which we will discuss briefly.

[48] Only the Big Bear aftershock (M6.1), which occurred approximately 3 hours after the main shock, was included in our calculation of initial stress and pore pressure fields. In Figure 5, large aftershocks ($M > 5.0$) are shown as blue squares. Many of these are located near clusters of smaller aftershocks which have decreasing pore pressure and negative initial Coulomb stress values. It may be that the stress and pore pressure perturbations due to these events must be added at the time of the event during simulation to get the correct pore pressure or Coulomb stress change tendency.

[49] There is a fairly large cluster of aftershocks to the north of the Big Bear epicenter which have positive coseismic Coulomb stress but decreasing pore pressure and decreasing Coulomb stress. *Jones and Hough* [1995] analyzed strong motion and TERRASCOPE data and concluded that the Big Bear event consisted of at least two subevents, one of which occurred along a northwest trending plane antithetical to the presumed Big Bear fault plane. This conclusion is supported by the significant aftershock activity along the both the presumed rupture plane and the antithetic fault plane. Furthermore, two large events, one a M5.2 preshock ~22 min before the Big Bear event and a M5.0

event ~6 weeks after the Big Bear event, would significantly alter the stress field as well as the pore pressure field near the Big Bear fault. Rupture on the antithetic fault plane, as well as the preshock and aftershock just mentioned, if included in our stress field calculations, might well account for the declining Coulomb stress that we calculated for the cluster of aftershocks north of the Big Bear fault.

[50] The permeability structure of fault zones can be anisotropic and heterogeneous. (See the collection of papers on this subject edited by *Hickman et al.* [1995].) A cluster of aftershocks is located within the fault zone, near the transfer region centered at latitude 34.5°. If the fault segments bounding this region have very low permeability normal to the fault, nonlinear effects such as the Mandel-Cryer effect described earlier could cause pore pressure and Coulomb stress to rise in this region even though the earthquake-induced pore pressure was high and would eventually decrease.

[51] Most of the aftershocks that occur where postseismic pore pressure or Coulomb stress are decreasing are located off the southwestern end of the Landers fault. In this complicated region several factors are not included in our stress evolution model. *Hough* [1993] concludes that the Eureka Peak fault, located south of the Landers epicenter, ruptured ~35 s after the main shock initiation. Then, approximately 2.5 min later, a large aftershock (M5.6) occurred located at 34.13°N, −116.40°W, which is indicated as a blue square in Figure 2. Comparing Figures 2 and 6, it is evident that many of the green aftershocks (pore pressure decreasing) are in regions where the pore pressure is relatively small and are near the Eureka Peak events. The regional stress modification caused by the M5.6 Eureka Peak aftershock is not included in the computation of stress and pore pressure in our model.

[52] We mention again that only the Joshua Tree, Landers, and Big Bear ruptures were included in our calculation of the initial stress field and pore pressure fields. Aftershocks of M5 or greater, of which there were 13 in the year following the Landers rupture, would have significant effect on the pore pressure very near the event. Many of the aftershocks for which the computed pore pressure was declining at the time of the event occur in clusters near the large aftershocks. For example, on 29 November and 4 December, two large aftershocks (M5.1 and M5.4) occurred just north of the Big Bear fault. A cluster of aftershocks was apparently spawned by these two events in a region where pore pressure was decreasing. The pore pressure field, however, would have been significantly altered by the relatively large aftershocks. A more accurate simulation would have to incorporate the stress and pore pressure changes for all moderately large events if it was to accurately model the actual pressure evolution of the region.

[53] *Booker* [1974] used the fully coupled Biot equations for poroelasticity to show that pore fluid diffusion following a fault dislocation causes partial reloading of the stress on the fault. Another way to interpret this poroelastic effect is that the presence of pore fluids in an elastic medium partially resists the stress imposed by the initial fault dislocation. Pore fluid acts as a ''shock absorber'' that mitigates, so some extent, the initial strain imposed by an earthquake rupture. The fluid flow that follows relaxes the resistance and the strain tends asymptotically toward the state that would have been attained initially if the fluid had not been present. We might expect, then, that pore fluid diffusion would tend to cause Coulomb stress to increase over time in locations where the initial Coulomb stress was positive. This is consistent with the results derived by *Jaume and Sykes* [1992]. Coulomb stress increases will tend to occur in regions where pore pressure is increasing, but the correspondence will not be exact, since the movement of fluid is controlled by permeability, which may be quite heterogeneous in the crust. This can explain why predictions of aftershock location based on initial static Coulomb stress calculations and on pore pressure change both give fairly good results.

6. Conclusions

[54] The time dependence of aftershocks requires a time-dependent physical mechanism. Since the crust is a fluid-saturated poroelastic medium in many locations, if not all, it is time-dependent behavior in terms of coupled poroelasticity must be examined. Fluid in the brittle crust causes the crust to exhibit diffusive relaxation after the sudden imposition of a dislocation, such as rupture on a fault. The fluid initially resists the stress in the material, then relaxes as fluid flows from regions of high pressure to regions of low pressure. The rate of relaxation and the flow paths taken by the fluid are controlled by the permeability of the material. Heterogeneous permeability can lead to unexpected behavior, such as rising pore pressure in pockets of low permeability surrounded by declining pore pressure. Since poroelastic materials exhibit time-dependent stress fields, we are led to examine whether or not this physical process is significant enough to explain the temporal patterns of aftershock sequences.

[55] Because there is ample evidence to suggest that the crust behaves as a poroelastic medium, it is reasonable to expect that pore fluid diffusion will have an effect on the stress state of the crust. Pore fluids initially resist imposed stresses, then relax over time. Theoretically, we have established that poroelasticity, which must apply to the crust, can account for the time delay in the onset of aftershocks. The fundamental remaining question is to determine whether or not the material properties of the crust and the amount of fluid present in crustal rocks, are sufficient to account for the actual observed aftershock sequences. This can only be established by comparing theoretical predictions with data. When the equations that describe a physical phenomenon are simple enough, back-of-the-envelope solutions to the governing equations are accurate enough to determine the appropriateness of the theory. Poroelastic dynamics, even with homogeneous material properties, is sufficiently complex that detailed computer simulation is required to determine if theory explains the data. Our simulations show that the majority of Landers aftershocks occurred where the Coulomb stress due to pore fluid diffusion was increasing. A considerably higher fraction of the aftershocks occur where the evolving poroelastic Coulomb stress is positive at the time of the aftershock than when the coseismic Coulomb stress alone is positive. The poroelastic explanation for the time dependence of aftershocks is not in conflict with previous work showing the high correlation between positive coseismic Coulomb stress

and aftershock locations, nor does it preclude the (likely) possibility that other effects discussed earlier are also active. Poroelastic materials behave in such a way that Coulomb stress tends to increase in many regions where the initial Coulomb stress was positive. This explains the reasonably good correlation between initial Coulomb stress and aftershocks and our present results.

[56] Since permeability controls the direction and rate of fluid diffusion in a porous medium, more accurate knowledge of the permeability structure in fault zones and the surrounding regions will be required to make better calculations of the rate and magnitude of poroelastic stress changes due to pore fluid movement. The pressure dependence of permeability, spatial heterogeneities and anisotropy in and near the fault zone may dramatically affect fluid flow patterns and the evolution of the postseismic pressure field. The magnitude of the poroelastic effect depends also on the elastic parameters of the material, particularly the difference between drained and undrained elastic moduli. Detailed and accurate fault models for the main shocks and aftershock focal mechanisms will also be needed to make more accurate determinations of the explanatory power of poroelasticity. Nevertheless, even approximate estimates for material parameters appear to be accurate enough to make reasonable simulations that support the poroelastic explanation for aftershocks.

[57] More simulations such as the one carried out in this study are needed to establish poroelastic relaxation as the cause of aftershocks. If quantitative models for rate and state friction can be incorporated into a poroelastic continuum simulation, it may be possible to use simulations to differentiate between competing effects by varying parameters. Similarly, viscoelastic relaxation of the lower crust can also be studied. These simulations await the development of a general earthquake modeling framework that will enable these rather complicated codes to be assembled.

[58] **Acknowledgments.** This work was supported by USGS/NEHERP grant 1434-HQ-97-GR-03 and DOE Basic Science Program grant FG03-86ER13601. The authors thank Egill Hauksson of the California Institute of Technology for generously supplying focal mechanisms for aftershocks of the 1992 Landers earthquake.

References

Biot, M. A., General solutions of the equations of elasticity and consolidation for a porous material, *J. Appl. Mech.*, *78*, 91–96, 1956.

Booker, J. T., Time dependent strain following faulting of a porous medium, *J. Geophys. Res.*, *79*, 2037–2044, 1974.

Bosl, W. J., and A. Nur, Numerical simulation of postseismic deformation due to pore fluid diffusion, in *Poromechanics: A Tribute to Maurice A. Biot*, edited by J.-F. Thimus, pp. 23–28, A. A. Balkema, Brookfield, Vt., 1998.

Bosl, W. J., and A. Nur, Modeling complex crustal processes, in *GeoComplexity and the Physics of Earthquakes*, *Geophys. Monogr. Ser.*, vol. 120, edited by J. B. Rundle, D. L. Turcotte, and W. Klein, AGU, Washington, D. C., 2000a.

Bosl, W. J., and A. Nur, Crustal fluids and earthquakes, in *GeoComplexity and the Physics of Earthquakes*, *Geophys. Monogr. Ser.*, vol. 120, edited by J. B. Rundle, D. L. Turcotte, and W. Klein, AGU, Washington, D. C., 2000b.

Charlez, P. A., *Rock Mechanics*, vol. 1, *Theoretical Fundamentals*, Editions Technip, Paris, 1991.

Cohee, B. P., and G. C. Beroza, Slip distribution of the 1992 landers earthquake and its implications for earthquake source mechanics, *Bull. Seismol. Soc. Am.*, *84*, 692–712, 1994.

Cryer, C. W., A comparison of the three-dimensional consolidation theories of Biot and Terzaghi, *Q. J. Mech. Appl. Math.*, *16*, 401–412, 1963.

Deng, J., M. Gurnis, H. Kanamori, and E. Hauksson, Viscoelastic flow in the lower crust after the 1992 Landers, california, earthquake, *Science*, *282*, 1689–1692, 1998.

Dieterich, J., A constitutive law for rate of earthquake production and its application to earthquake clustering, *J. Geophys. Res.*, *99*, 2601–2618, 1994.

Gomberg, J., and S. Davis, Stress/strain changes and triggered seismicity at The Geysers, California, *J. Geophys. Res.*, *101*, 733–749, 1996.

Gomberg, J., M. Blanpied, and N. M. Beeler, Transient triggering of near and distant earthquakes, *Bull. Seismol. Soc. Am.*, *87*, 294–309, 1997.

Gross, S., and C. Kisslinger, Estimating tectonic stress rate and state with Landers aftershocks, *J. Geophys. Res.*, *102*, 7603–7612, 1997.

Hardebeck, J. L., J. J. Nazareth, and E. Hauksson, The static stress change triggering model: Constraints from two southern California aftershock sequences, *J. Geophys. Res.*, *103*, 24,427–24,437, 1998.

Harris, R. A., Introduction to special section: Stress triggers, stress shadows, and implications for seismic hazard, *J. Geophys. Res.*, *103*, 24,347–24,358, 1998.

Hickman, S., R. Sibson, and R. Bruhn (Eds.), *The Mechanical Involvement of Fluids in Faulting*, U.S. Geol. Surv., Menlo Park, Calif., 1994.

Hickman, S., R. Sibson, and R. Bruhn, Introduction to special section: The mechanical involvement of fluids in faulting, *J. Geophys. Res.*, *100*, 12,831–12,840, 1995.

Hough, S. E., Southern surface rupture associated with the 1992 *M*7.4 Landers earthquake; Did it all happen during the mainshock?, *Geophys. Res. Lett.*, *20*, 2615–2618, 1993.

Hubbert, M. K., and W. W. Rubey, *Geol. Soc. Am. Bull.*, *70*, 1959.

Hudnut, K. W., et al., Co-seismic displacements of the 1992 Landers earthquake sequence, *Bull. Seismol. Soc. Am.*, *84*, 625–645, 1994.

Jaume, S. C., and L. R. Sykes, Changes in state of stress on the southern San Andreas fault resulting from the California earthquake sequence of April to June 1992, *Science*, *258*, 1325–1328, 1992.

Jones, L. E., and S. E. Hough, Analysis of broadband records from the 28 June 1992 Big Bear earthquake: Evidence of a multiple-event source, *Bull. Seismol. Soc. Am.*, *85*, 688–704, 1995.

King, G. C. P., R. S. Stein, and J. Lin, Static stress changes and the triggering of earthquakes, *Bull. Seismol. Soc. Am.*, *84*, 935–953, 1994.

Langtangen, H. P., *Computational Partial Differential Equations*, Springer-Verlag, New York, 1999.

Larsen, S. C., Geodetic measurements of deformation in southern california, Ph.D. thesis, Calif. Inst. of Technol., Pasadena, 1991.

Li, V. C., S. H. Seale, and T. Cao, Postseismic stress and pore pressure readjustment and aftershock distributions, *Tectonophysics*, *144*, 37–54, 1987.

Mavko, G., T. Mukerji, and J. Dvorkin, *The Rock Physics Handbook*, Cambridge Univ. Press, New York, 1998.

Nur, A., and J. R. Booker, Aftershocks caused by pore fluid flow?, *Science*, *175*, 885–887, 1972.

Peltzer, G., P. Rosen, F. Rogez, and K. Hudnut, Postseismic rebound in fault step-overs caused by pore fluid flow, *Science*, *273*, 1202–1204, 1996.

Peltzer, G., P. Rosen, and F. Rogez, Poroelastic rebound along the Landers 1992 earthquake surface rupture, *J. Geophys. Res.*, *103*, 30,131–30,145, 1998.

Richter, C., *Elementary Seismology*, W. H. Freeman, New York, 1958.

Roeloffs, E., Poroelastic techniques in the study of earthquake-related hydrologic phenomena, *Adv. Geophys.*, *37*, 135–195, 1996.

Rundle, J. B., W. Klein, and S. Gross, Physical basis for statistical patterns in complex earthquake populations: Model, predictions, and tests, *Pure Appl. Geophys.*, *155*, 575–607, 1999.

Savage, J. C., and W. H. Prescott, Asthenosphere readjustment and the earthquake cycle, *J. Geophys. Res.*, *83*, 3369–3376, 1978.

Scholz, C. H., *The Mechanics of Earthquakes and Faulting*, Cambridge Univ. Press, New York, 1990.

Seeburger, D. A., Studies of natural fractures, fault zone permeability, and a pore space-permeability model, Ph.D. thesis, Stanford Univ., Stanford, Calif., 1981.

Sleep, N. H., Ductile creep, compaction, and rate and state dependent friction within major fault zones, *J. Geophys. Res.*, *100*, 13,065–13,080, 1995.

Wald, D. J., and T. H. Heaton, Spatial and temporal distribution of slip for the 1992 Landers, California, earthquake, *Bull. Seismol. Soc. Am.*, *84*, 668–691, 1994.

Wang, H. F., Quasi-static poroelastic parameters in rock and their geophysical applications, *Pure Appl. Geophys.*, *141*, 269–286, 1993.

Yeats, R. S., K. Sieh, and C. R. Allen, *The Geology of Earthquakes*, Oxford Univ. Press, New York, 1997.

W. J. Bosl and A. Nur, Geophysics Department, Stanford University, Stanford, CA 94305-2215, USA. (bosl@pangea.stanford.edu)

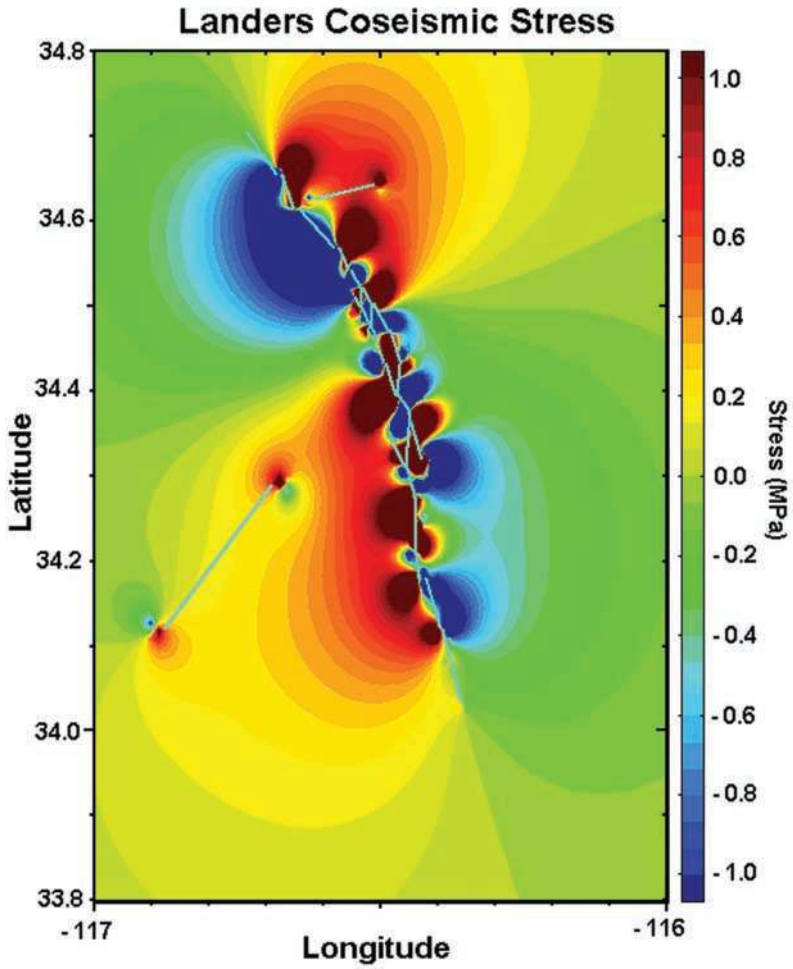

Figure 1. Coseismic mean stress field computed from *Hudnut et al.* [1994] slip model. Fault trace is superimposed on the mean stress image. Negative mean stress is compressive. Initial pore pressure distribution is computed directly from this.

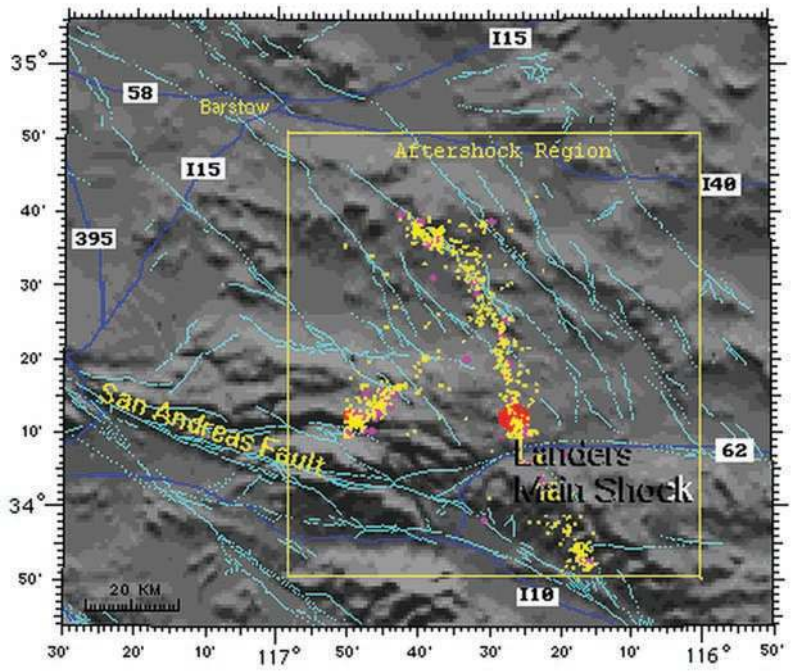

Figure 3. Sketch of the Mojave region where the Landers earthquake occurred. The yellow box outlines the region over which aftershock events were counted for this study.

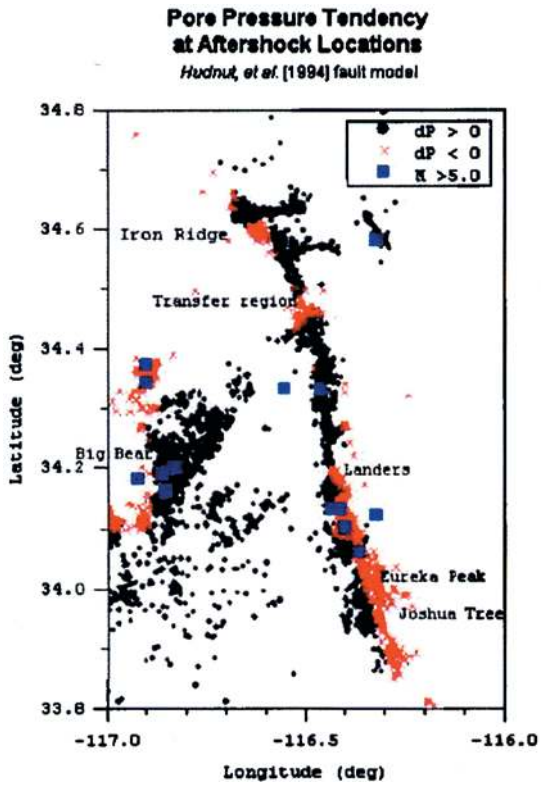

Figure 5. Locations of all $M > 2.0$ aftershocks in the 1-year period following the Landers earthquake are shown. Black dots indicate events that occur where the pore pressure has increased since the main shock, and red crosses indicate events where pore pressure has decreased. Large aftershocks ($M > 5.0$) are shown as blue squares.

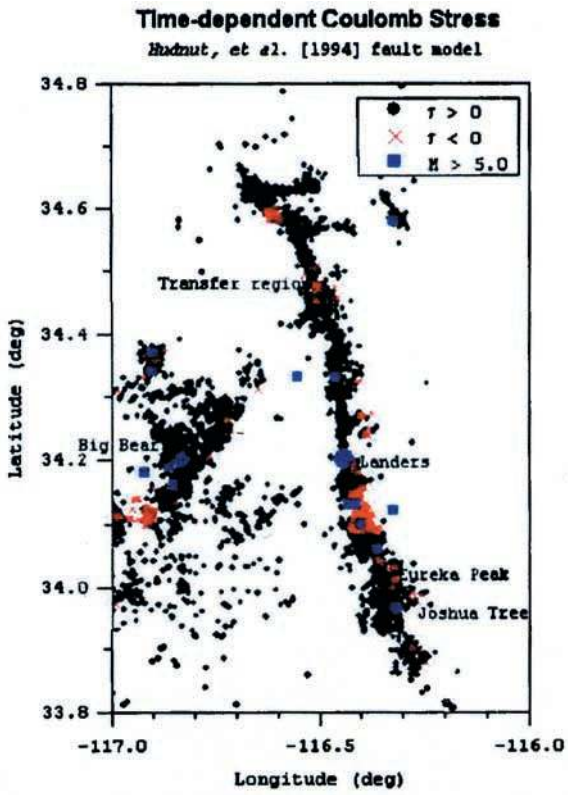

Figure 6. Locations of all $M > 2.0$ aftershocks in the 1-year period following the Landers earthquake are shown. Black dots indicate events that occur where the total Coulomb stress is positive, and red crosses indicate events where it is negative at the time of the event. Large aftershocks ($M > 5.0$) are shown as blue squares. Black dots ($\tau(t) > 0$) represent 86% of the aftershocks.

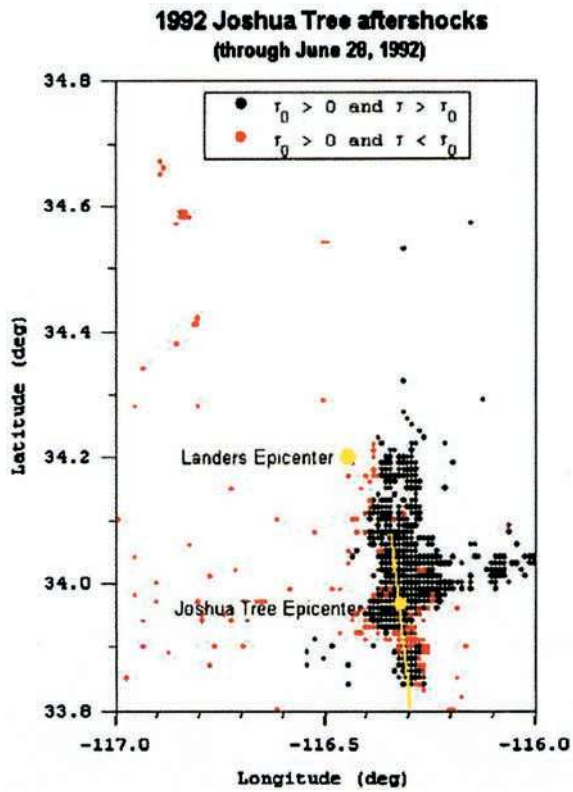

Figure 7. Locations of all $M > 2.0$ aftershocks in the 3-month period (23 April to 28 June) following the Joshua Tree earthquake are shown. Black dots indicate events that occur where the total Coulomb stress is positive, and red crosses indicate events where it is negative at the time of the event. Black dots ($\tau(t) > 0$) represent 95% of the aftershocks.